Università degli studi di Padova
Dipartimento di Fisica e Astronomia

Tesi di Dottorato

Search for heavy resonances decaying into a Z boson and a vector boson in the $\nu\bar{\nu}\,q\bar{q}$ final state at CMS

Supervisor: Prof. Franco Simonetto
Candidate: Lisa Benato

Scuola di Dottorato di Ricerca, XXX ciclo

"I have no special talent. I am only passionately curious."
(A. Einstein)

Contents

1

Abstract

2

3

Chapter

1

Introduction

Chapter

2

Theoretical motivation

Chapter

3

The Large Hadron Collider and the CMS experiment

Chapter

4

Search for diboson resonances in the $ZV \to \nu\bar{\nu}q\bar{q}$ final state

4.1 Analysis overview

This analysis searches for signal of heavy resonances decaying into a pair of heavy vector bosons, using the data collected by the CMS experiment during 2016, for an integrated luminosity of $\mathcal{L} = 35.9\ \text{fb}^{-1}$. One Z boson is identified through its invisible decay ($\nu\nu$), while the other boson, labelled as V and consisting either as a W or a Z boson, is required to decay hadronically into a pair of quarks. The decay products (the bosons) of heavy (around the TeV scale) resonances are produced with large Lorentz boosts; as a consequence, the decay products of the bosons (quarks and neutrinos) are expected to be highly energetic and collimated. In this regime, the standard jet reconstruction algorithms fail in distinguishing the two jets from the quarks, suggesting to look for a signature composed of a large-cone high-p_T jet, in which both q and $\bar{q}$ lie, recoiling against a large amount of missing transverse energy ($\vec{p}_T^{\,\text{miss}}$) due to the neutrinos escaping the detector. The hadronically decaying boson (Z, W) is then reconstructed as one large-cone jet, whose mass is used to define the signal region and signal-depleted control regions, the sidebands. Jet substructure techniques are exploited in order to suppress background contamination and to classify the events in two exclusive signal purity categories, allowing to improve the discovery reach.

A ZZ final state, predicted by the bulk graviton model (sec. **??**), can be reconstructed in channels with high purity but limited statistics (four charged leptons) and large statistics but overwhelming backgrounds (no charged leptons). The choice to look for one boson decaying hadronically and the other Z into neutrinos represents the best compromise between these two extremes. This topology can be also utilized to reconstruct a charged spin-1 vector boson decaying into an invisible Z and a hadronic W, predicted by HVT model (sec. **??**), making this analysis sensitive to a generic VZ final state.

Signal events are collected with trigger paths requiring high $\vec{p}_T^{\,\text{miss}}$ recoiling against jet activity. This signature is clearly a very challenging one in an environment with more than 50 primary collisions per bunch crossing. For this reason, the Particle-Flow algorithm is run at trigger level to obtain the highest possible resolution on the jets and thus on the $\vec{p}_T^{\,\text{miss}}$.

The search is performed by examining the distribution of the diboson reconstructed transverse mass of the resonance VZ (m_{VZ}^T) for a localized excess. The shape and normalization of the main

background of the analysis (namely, the production of an electroweak boson in association with jets) are estimated with a data-simulation hybrid approach using the distribution of data in the sidebands, corrected for a function accounting for potential differences between the signal region and the sidebands, while the minor background sources are taken from simulations.
In fig. 4.1, a typical signal event of the $W' \to WZ \to q\bar{q}'\nu\bar{\nu}$ process detected by the CMS experiment is displayed; the mass of the W' is 2.5 TeV. The muon chambers in the barrel (DTs, in light red) and in the endcaps (CSCs, in light blue), along with the tracker detector (green) are shown in the (r,ϕ) transverse plane (left) and the (r,z) longitudinal plane (right). The large-cone jet, identifying the W hadronic decay, is displayed in red; the energy deposits in ECAL (light orange) and in HCAL (in violet) can be seen in the picture. The missing transverse energy, signature of the Z invisible decay, is represented as a blue arrow, lying in the transverse plane. The track multiplicity (green tracks) is shown in the center of the detector, where the tracker is installed.

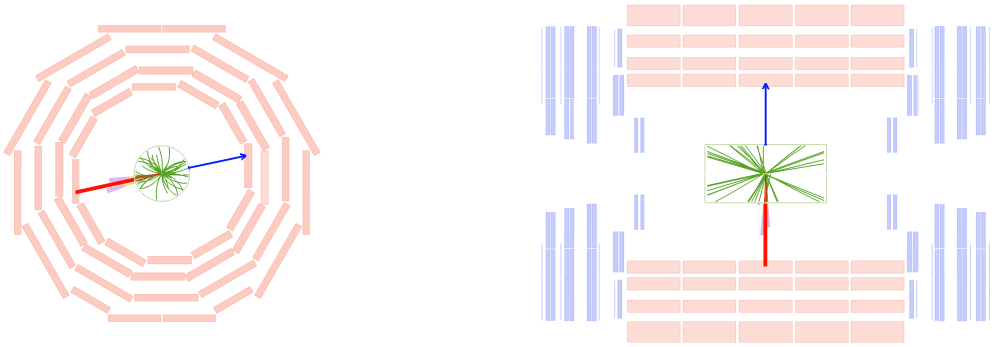

Figure 4.1: Left: representation of the decay of a W' of mass 2.5 TeV, in the transverse plane of the CMS detector. Right: representation of the decay of a W' of mass 2.5 TeV, in the longitudinal plane of the CMS detector.

4.2 Event selection

In this section, a list of the selections applied to the physics objects used in the analysis is presented, together with performance and validation plots.

4.2.1 Vertex and Pile-up

Due to the pile-up effect, several primary vertices are typically reconstructed in an event. The primary vertex of the event is defined as the one with the highest sum of transverse momenta $\sum p_T^2$ of clustered physics objects associated to it, which passes the following selections:

- number of degrees of freedom $N_{DoF} > 4$
- vertex position along the beampipe $|z_{vtx}| < 24$cm
- vertex distance with respect the beam pipe $d_0 < 2$cm

where z_{vtx} and d_0 are the distance along and perpendicular to the beam line of the vertex with respect the nominal interaction point $(0,0,0)$.
The Monte Carlo samples listed in sec. **??** are generated simulating the pile-up conditions, as expected in the 25 ns bunch crossing pile-up scenario. Nevertheless, the MC pile-up description does

not match exactly the conditions in data, and there is therefore the need to reweight the simulated events in order to improve the agreement with the data.
The MC samples are reweighted assuming a total inelastic cross section of $\sigma_{in} = 69200\mu b$. The comparison between the distributions of primary vertices in data and MC after the pile-up reweighting is applied is shown in fig. 4.2 for an event selection (called inclusive selection) requiring large amount of $\vec{p}_T^{\,\text{miss}}$ recoiling against an AK8 fat jet (tab. **??**).

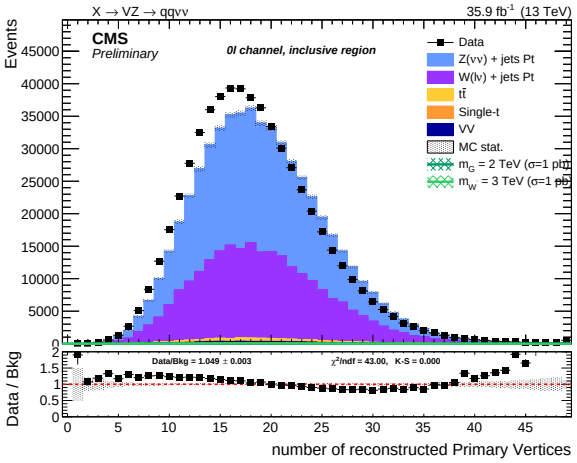

Figure 4.2: Primary vertices distributions in data and MC samples, after reweighting.

4.2.2 Electrons

Electrons used in this analysis, reconstructed from energy deposits in the ECAL matched to tracks reconstructed in the silicon tracker, are required to pass the Particle-Flow criteria, and to fall in the ECAL pseudorapidity fiducial range ($|\eta| < 2.5$). The electron identification is defined with a "cut-based" approach. In the isolation definition the effect of pile-up is considered by taking into account the energy deposits in the calorimeter, estimated through the so-called ρ*-area* method, by subtracting the median energy density in the event ρ multiplied by electron effective area. The isolation value is computed in a ΔR cone of 0.3 centered along the lepton direction.
Since in this analysis aims at a final state without any lepton, every electron identified with the looser cut-based criteria (*veto Id*), transverse momentum $p_T > 10$ GeV is vetoed. The detailed set of cuts to define a *veto* cut-based Id electron are reported in tab. 4.1; this set of selctions allow to identify an electron with an efficiency of $\sim 95\%$. The supercluster width is indicated as $\sigma_{i\eta i\eta}$; $\Delta\eta_{in}^{seed}$ and $\Delta\phi_{in}$ are the difference in η and ϕ between the track position as it is measured in the inner layer, and then extrapolated to the interaction vertex and to the calorimeter, and the η of the seed cluster or the ϕ of the supercluster; H/E is the hadronic leakage, *i.e.* the ratio of the hadronic energy of the calorimetric towers to the electromagnetic energy of the electron supercluster; *relIso* indicates the relative isolation calculated with the effective area approach; $1/E - 1/p$ is the difference of the inverse of the energy and the momentum; d_0 and d_z are the transverse and longitudinal impact parameters. A dedicated conversion veto is applied to mitigate the effects of electrons undergoing bremsstrahlung in the silicon detector.

4.2.3 Photons

As in the case of electrons, a photon veto is applied in the analysis both for the signal and the control regions. Events are rejected if they contains one (or more) photon with $p_T > 15$ GeV , $|\eta| < 2.5$, pass-

Electrons		Veto	
		EB	EE
$\sigma_{i\eta i\eta}$	<	0.0115	0.037
$\Delta\eta_{in}^{seed}$	<	0.00749	0.00895
$\Delta\phi_{in}$	<	0.228	0.213
H/E	<	0.356	0.211
relIso (Effective Area)	<	0.175	0.159
$\lvert 1/E - 1/p \rvert$	<	0.299	0.15
$\lvert d_0 \rvert$	<	0.05	0.10
$\lvert d_z \rvert$	<	0.10	0.20
missing hits	≤	2	3
conversion veto		yes	yes

Table 4.1: Electron cut-based selection for 25 ns bunch spacing conditions. EB: barrel cuts ($|\eta_{\text{supercluster}}| \leq 1.479$); EE: endcap cuts ($|\eta_{\text{supercluster}}| > 1.479$)

ing the Loose cut-based photon Id, whose definition is reported in tab. 4.2. The isolation cuts (using the rho-area method for the mitigation of the pileup) and conversion safe electron veto are applied. The isolation value is computed in a ΔR cone of 0.3 and is corrected for pileup by subtracting the event-by-event energy density (ρ) times an effective area.

Photons		Loose	
		EB	EE
H/E	<	0.0597	0.0481
$\sigma_{i\eta i\eta}$	<	0.01031	0.03013
PF ch.had.iso.(ρ-corr)	<	1.295	1.011
PF neu.had.iso.(ρ-corr)	<	$10.910 + 0.0148 p_T + 0.000017 p_T^2$	$5.931 + 0.0163 p_T + 0.000014 p_T^2$
PF photon iso.(ρ-corr)	<	$3.630 + 0.0047 p_T$	$6.641 + 0.0034 p_T$
conversion veto		yes	yes

Table 4.2: Photon cut-based selection for 25 ns bunch spacing conditions. EB: barrel cuts ($|\eta_{\text{supercluster}}| \leq 1.479$); EE: endcap cuts ($|\eta_{\text{supercluster}}| > 1.479$)

4.2.4 Muons

The minimal criteria to define a muon is that it must be identified by the Particle-Flow algorithm, and should be reconstructed either as a global muon or as a tracker muon (sec. **??**). The muon isolation is defined in cone with a radius of $\Delta R = 0.4$ centered along the lepton direction. In the analysis event selection, all muons identified with the loosest criteria previously described, p_T over 10 GeV, PF isolation below 0.25, $\eta < |2.4|$ are vetoed.

4.2.5 Taus

The presence of hadronically-decaying taus only act as veto for the events both in the signal and in the control regions to suppress electroweak backgrounds. The selection criteria for taus are $p_T > 18$ GeV and $|\eta| < 2.3$. Loose identification criteria of the hadronic tau reconstruction algortihms are required and applied in order to identify possible tau candidates.

4.2.6 Jets

In this analysis, jets are considered if the corrected p_T is larger than 30 GeV for AK4 jets and 200GeV for AK8 jets, and lie in the tracker acceptance ($|\eta| < 2.4$). Additionally, AK4 jets are required to pass *loose* jet identification requirements, AK8 are required to pass *tight* jet identification requirements defined in tab. 4.3. AK8 jets are used to reconstruct the hadronically decaying electroweak boson candidate, whilst AK4 jets are used to suppress the contribution of top and QCD background events. Jet energy corrections are applied to AK4 and AK8 CHS jets. Fig. 4.3- 4.5 show the data/simulation comparison after the analysis selections (tab. **??** without Top cleaning and Event cleaning).

PF Jet ID	*loose*	*tight*
Neutral Hadron Fraction	< 0.99	< 0.90
Neutral EM Fraction	< 0.99	< 0.90
Number of Constituents	> 1	> 1
Muon Fraction	-	-
Additionally, for $\|\eta\| < 2.4$		
Charged Hadron Fraction	> 0	> 0
Charged Multiplicity	> 0	> 0
Charged EM Fraction	< 0.99	< 0.99

Table 4.3: *Loose* and *Tight* jet identification requirements for 25 ns bunch spacing conditions.

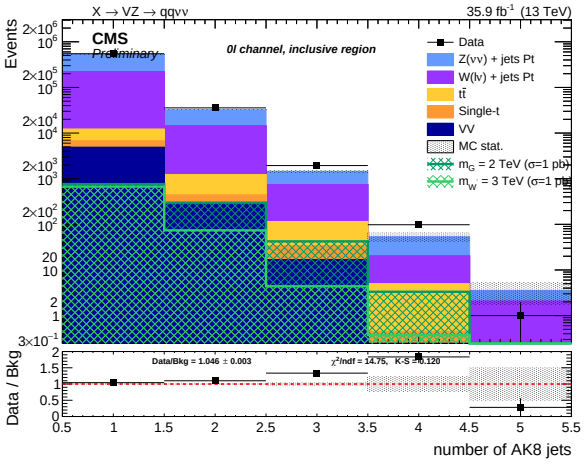

Figure 4.3: Number of reconstructed AK8 jets after selections.

Since it has been measured that the jet energy resolution (JER) is not the same in data and MC, an additional smearing is applied in simulation, in order to get a better agreement. There are two independent ways to get the smearing. The scaling method rescales the corrected four-momentum of a reconstructed jet by a factor

$$c_{\mathrm{JER}} = 1 + (s_{\mathrm{JER}} - 1)\frac{p_T - p_T^{\mathrm{gen}}}{p_T}, \tag{4.1}$$

where p_T is the transverse momentum of the jet, p_T^{gen} is the transverse momentum of the generator level particle corresponding to the reconstructed jet, and s_{JER} is the data-simulation resolution scale

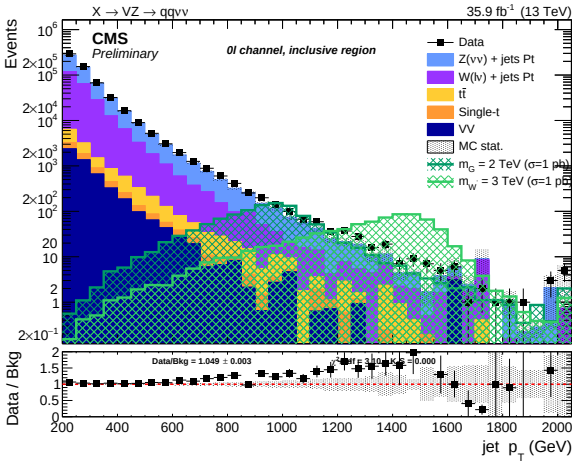

Figure 4.4: Leading AK8 jet p_T spectra after selections.

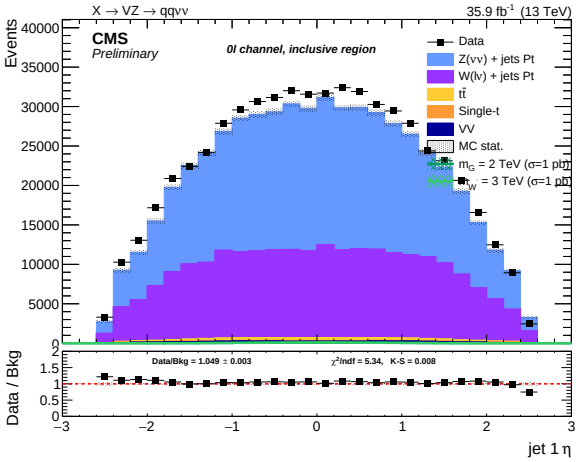

Figure 4.5: Leading AK8 jet η spectra after selections.

factor. The factor c_{JER} is positively defined, hence if negative it is set equal to zero. The generator level particle and a reconstructed jet are defined as matched if:

$$\Delta R < R_{\text{cone}}/2, |p_T - p_T^{\text{ptcl}}| < 3\sigma_{\text{JER}} p_T, \tag{4.2}$$

where R_{cone} is the jet clustering parameter and σ_{JER} is the relative p_T resolution measured in simulation.

The alternative approach is the stochastic smearing, and it does not require the matching with the generator level particle. The jet four-momentum is rescaled by a factor

$$c_{\text{JER}} = 1 + \mathcal{N}(0, \sigma_{\text{JER}}) \sqrt{max(s_{\text{JER}}^2 - 1, 0)}, \tag{4.3}$$

where σ_{JER} is the relative p_T resolution in simulation, s_{JER} is the data-simulation scale factor, and $\mathcal{N}(0,\sigma)$ is a random number extracted from a gaussian normal distribution, whose mean is zero and variance σ^2. Scaling factor c_{JER} is positively defined.

The smearing procedure adopted in this analysis is the hybrid method: when a matching jet at generator level is found, the scaling method is adopted, else the stochastic smearing is chosen. The smearing coefficients (scale factors, SF) as a function of the jet η and their uncertainties are reported in tab. 4.4 for 2016 data.

Jet η	Smearing SF
$0.0-0.5$	1.109 ± 0.008
$0.5-0.8$	1.138 ± 0.013
$0.8-1.1$	1.114 ± 0.013
$1.1-1.3$	1.123 ± 0.024
$1.3-1.7$	1.084 ± 0.011
$1.7-1.9$	1.084 ± 0.011
$1.9-2.1$	1.140 ± 0.047
$2.1-2.3$	1.067 ± 0.053
$2.3-2.5$	1.177 ± 0.041
$2.5-2.8$	1.364 ± 0.039
$2.8-3.0$	1.857 ± 0.071
$3.0-3.2$	1.328 ± 0.022
$3.2-5.0$	1.16 ± 0.029

Table 4.4: Data-simulation jet smearing coefficients and their corresponding uncertainties.

4.2.7 Jet mass

The jet mass is the main observable in distinguishing a V jet from a jet produced by colour interaction (QCD jets). Jet grooming procedure consists in the suppression of uncorrelated underlying event, pile-up and soft radiation from the jet and improves the discrimination, by pushing the jet mass for QCD jets towards lower values while maintaining the jet mass for V-jets around the electroweak boson mass window.
The grooming technique of the analysis relies on the "soft drop declustering" algorithm, a jet substructure technique which recursively removes soft wide-angle radiation from a jet [1], in order to mitigate the contaminations from initial state radiation, along with pile-up, multiple scatterings. The soft drop algorithm depends on two parameters: a soft threshold z cut and an angular exponent β. Starting with a jet of radius R_0 with only two constituents, the soft drop algorithm removes the soft constituent unless:

$$\frac{\min(p_T^1, p_T^2)}{p_T^1 + p_T^2} > z_{cut} \left(\frac{\Delta R_{12}}{R_0} \right)^{\beta}. \tag{4.4}$$

The degree of jet grooming is controlled by z_{cut} and β; if $\beta \to \infty$ the jet remains ungroomed. The $\beta = 0$ limit of the energy loss is particularly interesting, since it is largely insensitive to the value of the strong coupling constant. The default parameters used by CMS are $\beta = 0$ and $z_{cut} = 0.1$.

The main grooming algorithm, soft drop, is used in association with PUPPI [2] in order to remove soft and wide-angle radiations and the pile-up contribution.
The default soft-drop + PUPPI jet mass suffers from a systematic shift from the expected value of about $\sim 10\%$, and some residual dependence on the jet p_T. Further corrections to the jet mass have been applied:

Gen: a p_T-dependent correction to account for a small shift in the generated vector boson mass, applied only on simulated samples

Reco: a p_T-dependent correction to the reconstructed jet mass, applied separately for jets in the barrel and endcaps regions.

Figure 4.7- 4.8 show the jet mass for W or Z bosons before and after the correction, without applying any cut on this variable.

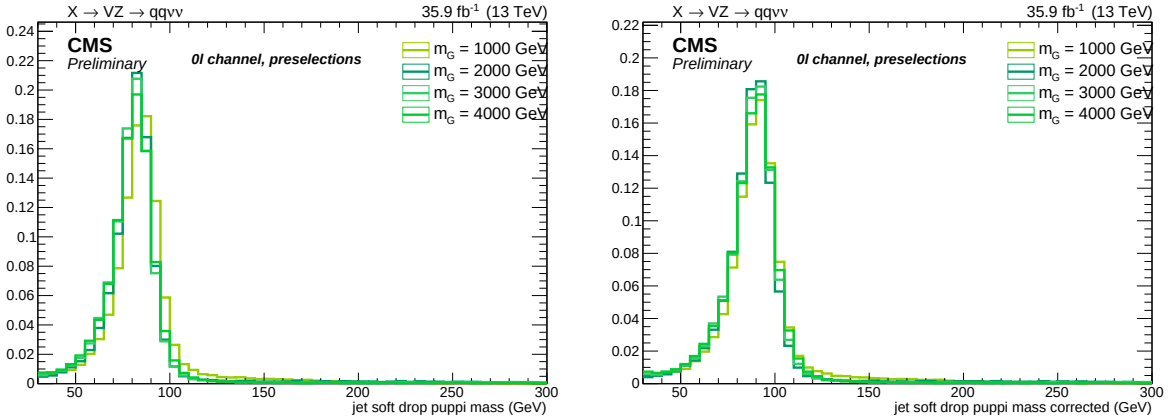

Figure 4.6: Softdrop + PUPPI mass of AK8 jet reconstructed for different bulk graviton signal samples; left: before corrections. right: after corrections.

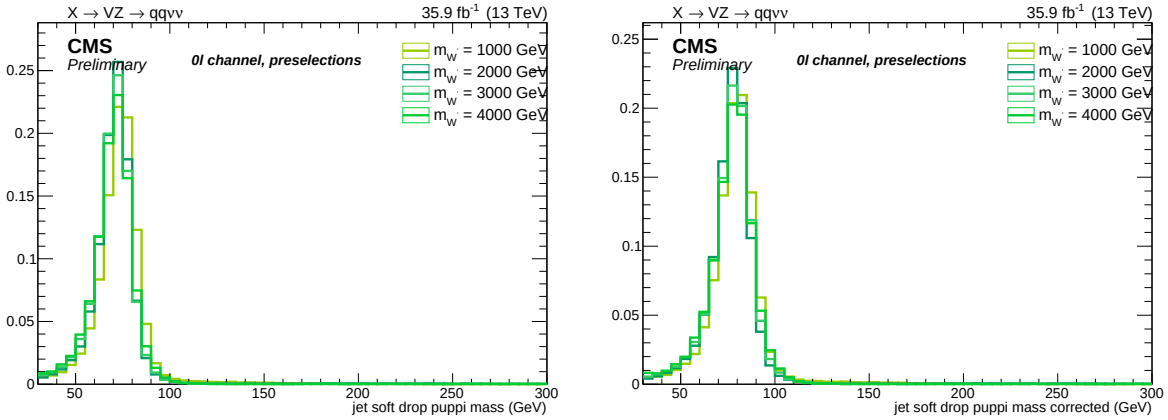

Figure 4.7: Softdrop + PUPPI mass of AK8 jet reconstructed for different $W^{'}$ signal samples; left: before corrections. right: after corrections.

In order to obtain a better data-Monte Carlo agreement, a smearing procedure has been applied to the soft drop + PUPPI jet mass, by using the stochastic method, with a constant smearing coefficent (1.00 ± 0.20), that does not depend on jet pseudorapidity if it is restricted to $|\eta| < 2.5$.

4.2.8 Jet substructure

In order to further discriminate signal from background, it useful to investigate the inner structure of the jet. Studying the distribution of the jet constituents with respect to the jet axis allows us to test the hypothesis of the existence of multiple substructures, that could be evidence of jets originated by

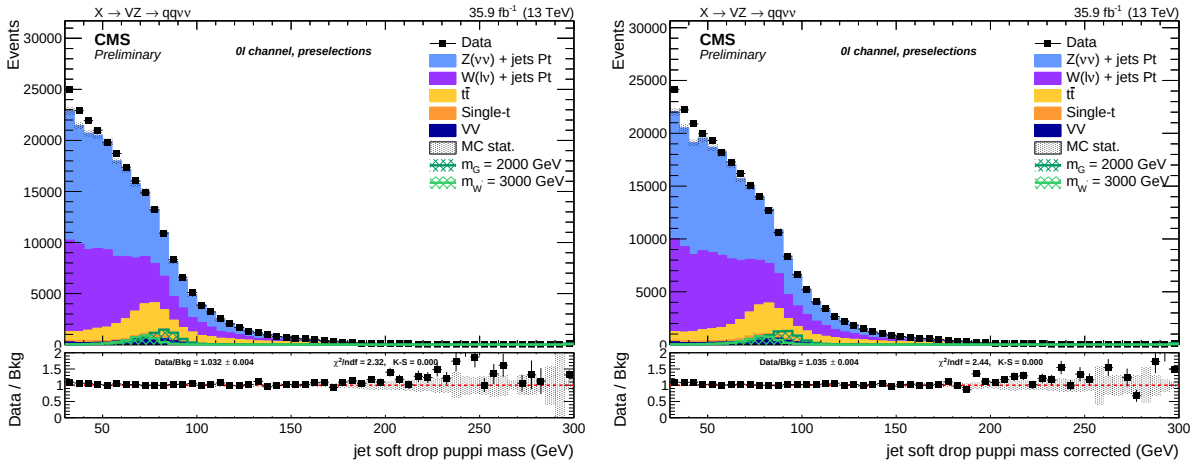

Figure 4.8: Softdrop + PUPPI mass of AK8 jet; left: before corrections. right: after corrections.

more than one parton. This procedure proceeds as follows: the constituents of the jet are clustered again with the k_T algorithm, however the procedure is stopped when one obtains N subjets. Then, a new variable, the N-subjectiness, is introduced. It is defined as:

$$\tau_N = \frac{1}{d_0}\sum_k p_{T,k} min(\Delta R^{\beta}_{1,k}, \Delta R^{\beta}_{2,k}, \ldots, \Delta R^{\beta}_{N,k})$$

where β is an arbitrary parameter, the index k runs over the jet constituents and the distances $\Delta R_{N,k}$ are calculated with respect to the axis of the N-th subjet, obtained by one iteration of τ minimization by varying the subjet axes around the k_T subjet axes.

The normalization factor d_0 is calculated as $d_0 = \sum_k p_{T,k} R_0^{\beta}$, setting R_0 to the radius of the original jet. The N-subjettiness is always included in the interval from 0 to 1 and represents the compatibility of the jet structure with an N-subjet hypothesis: small values correspond to high compatibility. Indeed, τ_N weights the transverse momentum of the jet constituents by their angular distance to the closest subjet. In this analysis the N-subjettiness is calculated from the ungroomed jet with the parameter $\beta = 1$. The subjettiness related to the one and two subjet hypothesis is thus:

$$\tau_1 = \frac{1}{d_0}\sum_k p_{T,k} \Delta R_{1,k}$$

and

$$\tau_2 = \frac{1}{d_0}\sum_k p_{T,k} min(\Delta R_{1,k}, \Delta R_{2,k})$$

In principle, these two quantities should allow us to distinguish the dipole-like nature of the showering of the Higgs decay from the classic monopole structure of QCD jets. In particular, the variable that best discriminates between V-jets and QCD jets is the ratio of 2-subjettiness and 1-subjettiness, $\tau_{21} = \tau_2/\tau_1$.

Figure 4.9 shows the τ_{21} distributions for the PUPPI algorithm.

Figure 4.9: τ_{21} subjettiness of PUPPI AK8 jet after inclusive selections.

4.2.9 b-tagging

B-tagging algorithms are applied to both the fat-jet and the sub-jets, independently. For subjets, run-II taggers are by default applied on the same charged particle-flow candidate list that is used in the jet clustering (*explicit jet-to-track association*). Thanks to the explicit jet-to-track association, the two sub-jets do not share any PF-constituent, avoiding unintended correlations.

The jet or sub-jet is considered as tagged if the discriminator value is above some threshold value, often referred to as the cut value, and the efficiency is defined as the number of jets which have a discriminator value that is above that cut divided by the total number of jets (of the same flavor).

The b-tagging algorithm used to set the analysis strategy is the Combined Secondary Vertex (CSV) [3] discriminator (full name `pfCombinedInclusiveSecondaryVertexV2BJetTags`). Different working points are provided by the POG for Run2 analyses [4], as shown in table 4.2.9, but the only one used in this analysis is the *loose* working point.

Working point	CSV cut	mis-tag probability
CSVL (Loose)	> 0.5426	$\approx 10\%$
CSVM (Medium)	> 0.8484	$\approx 1\%$
CSVT (Tight)	> 0.9535	$\approx 0.1\%$

Table 4.5: Working point for CSV b-tagging algorithm.

B-tagging efficiency is not the same in data and MC. In order to take into account this difference, the BTV POG provides collections of b-tagging scale factors for b-jets and mistagged light jets, measured for different physics processes, for the supported tagging algorithms and the three standard working points [3]. A weight is calculated on a per-event basis as a function of the b-tagging status of the jets and their kinematic variables [5].

In this analysis, b-tagging is used in order to reject events where a top quark is involved, by asking to the AK4 jets not laying in the AK8 jet cone to be anti b-tagged (in practice, the maximum CSV value allowed is the loose working point, CSVL).

4.2.10 Missing Energy

How the MET is reconstructed

The E_T^{miss} is the imbalance in the transverse momentum of all visible particles, and it is reconstructed with the particle flow algorithm [6]. The *raw* E_T^{miss} is defined as the inverse vectorial sum of the transverse momentum of all the reconstructed charged and neutral particle flow candidates: $\vec{E}_T^{\text{miss}} = -\sum_{i=0}^{all} \vec{p}_{T\,i}$. The raw E_T^{miss} is systematically different from true E_T^{miss}, for many reasons including the non-compensating nature of the calorimeters and detector misalignment. To better estimate the true E_T^{miss}, corrections can be applied:

Type-0: a mitigation for the degradation of the E_T^{miss} reconstruction due to the pileup interactions, by applying the CHS algorithm. However, the E_T^{miss} contribution from pileup neutral particles cannot be easily subtracted; the assumption is that the E_T^{miss} contribution term of charged and neutral pileup particles are the same, and cancellation at the true level is exact:An additional E_T^{miss} term is then added to the raw E_T^{miss} to take into account the neutral PU contribution, which is equal to the charged one with a multiplicative scale factor taking into account calorimeter mismeasurements of low-p_T energy deposits.

Type-1: propagation of the jet energy corrections (JEC) to MET. The Type-I correction replaces the

vector sum of transverse momenta of particles which can be clustered as jets with the vector sum of the transverse momenta of the jets to which JEC is applied.

Particle flow E_T^{miss} with type-1 corrections applied is currently the default one used by CMS physics analyses. Additionaly, some E_T^{miss} filters have been recommended by JETMET POG for Run2 analyses [7], in order to remove events with spurios E_T^{miss} related to detector noise and bad reconstructions.

- `HBHENoiseFilter`
- `HBHENoiseIsoFilter`
- `EcalDeadCellTriggerPrimitiveFilter`
- `goodVertices`
- `eeBadScFilter` (not recommended for Monte Carlo, hence not applied)
- `globalTightHalo2016Filter`
- `BadPFMuonFilter`
- `BadChargedCandidateFilter`

Since the E_T^{miss} corrections and uncertainties depend on the JEC applied, they are re-computed accordingly following the JETMETPOG recommendation:

```
from PhysicsTools.PatUtils.tools.runMETCorrectionsAndUncertainties import
runMetCorAndUncFromMiniAOD
# If you only want to re-correct and get the proper uncertainties
runMetCorAndUncFromMiniAOD(process,
                           isData=True (or False),
                           )
process.p = cms.Path(process.fullPatMetSequence *
   process.yourAnalyzer)

cms.InputTag("slimmedMETs","","YourProcessName")
```

Figure 4.10 show the E_T^{miss} distribution for data and Monte Carlo after the corrections and filters.

Figure 4.10: Type-1 corrected E_T^{miss} distribution after inclusive selections.

Chapter

5

Conclusions

Plot di Clemens

Bibliography

[1] A. J. Larkoski, S. Marzani, G. Soyez and J. Thaler, *Soft Drop*, *JHEP* **05** (2014) 146, [1402.2657].

[2] D. Bertolini, P. Harris, M. Low and N. Tran, *Pileup per particle identification*, *Journal of High Energy Physics* **2014** (2014) 59.

[3] CMS Collaboration, S. Chatrchyan et al., *Identification of b-quark jets with the CMS experiment*, *JINST* **8** (2013) P04013, [1211.4462].

[4] CMS Collaboration, *BTV POG - B-tagging for Run2 - https://twiki.cern.ch/twiki/bin/view/CMS/BtagRecommendation80X*, .

[5] *Methods to apply b-tagging efficiency scale factors*, 2013.

[6] CMS Collaboration, CMS Collaboration, *Particle-flow event reconstruction in CMS and performance for jets, taus, and* E_T^{miss}, .

[7] CMS Collaboration, *JetMET POG - Jet ID for Run2 - https://twiki.cern.ch/twiki/bin/view/CMS/JetID*, .